

# Spin transport and imaging opportunities in inhomogeneous environments

V. P. Bhallamudi,<sup>1</sup> A. J. Berger,<sup>2</sup> D. E. Labanowski,<sup>1</sup> D. Stroud,<sup>2</sup> and P. C. Hammel<sup>2,\*</sup>

<sup>1</sup>*Department of Electrical and Computer Engineering,  
The Ohio State University, Columbus, Ohio 43210, USA*

<sup>2</sup>*Department of Physics, The Ohio State University, Columbus, Ohio 43210, USA*  
(Dated: June 13, 2022)

Understanding and controlling spin-polarized transport in heterogeneous magnetic environments is essential for advancing spin-based electronics. Such transport is governed by a drift-diffusion equation; here we present a method of solving this equation even in the presence of a strongly inhomogeneous magnetic field and spatially varying spin lifetimes. Our approach elucidates global Hanle measurements and suggests the use of a scanned magnetic dipole for nanoscale imaging. Furthermore, magnetic field inhomogeneity is increasingly important, particularly in the vicinity of ferromagnets used to inject and detect spin magnetization. We present numerical analysis that sheds light on recent experimental observations.

PACS numbers: 75.76.+j, 75.40.Gb, 85.75.-d, 75.78.-n

Spin electronics is a rich and rapidly growing field that integrates magnetic and nonmagnetic materials to enable a variety of spin polarized transport phenomena [1, 2]. Central to this field is the preservation of spin polarization in the often complex magnetic environment that prevails in spin electronic (spintronic), particularly electrically injected, devices. Much progress has been made in understanding injection of spins into non-magnetic semiconductors, the manipulation of those spins within the semiconductor, and both local and global detection of the spin states [3–6]. Several recent results have brought us closer to electrically-controlled room-temperature spintronic devices [7–13]. The drift-diffusion equation governs spin transport, but is difficult to solve for a general, spatially dependent magnetic field as found in many spintronic devices. Here we report a method for solving this equation and present solutions to two important cases. We model spin transport in the presence of a magnetic dipole, which often accurately describes the tip of a magnetic scanned probe. By using such a probe, we show that it is possible to image local spin properties of a spin injected system (even in a global detection scheme). We further calculate the impact of injector fringing fields (unavoidably inhomogeneous on the nanoscale) on spin polarization in an adjacent nonmagnetic material.

Understanding the mechanisms that degrade spin polarization in the context of multicomponent spintronic devices is a topic of keen scientific and technological interest. A primary approach to measuring the spatial length and time scales over which spin polarization decays is to measure the dependence of spin transport on an applied magnetic field; these data are analyzed using the drift-diffusion equation. However, such analyses have been largely confined to uniform magnetic fields. Recent experiments demonstrate the inadequacy of this assumption, implicating inhomogeneous magnetic field effects [14, 15]. Here we present a comprehensive and very general framework for treating spins diffusing through a

medium with inhomogeneities of the field, lifetime, or diffusion constant, regardless of injection technique (e.g., optically using circularly polarized photons [16], or electrically from ferromagnetic contacts [5, 9, 11, 13, 17–19]).

We first describe an analytical method used to solve the spin diffusion equation for a uniform field with arbitrary orientation and discuss Hanle measurements in the presence of such fields. Next, we present a generalized numerical technique for dealing with inhomogeneities. Finally, we discuss these results and their expected implications for experiments.

Spin dynamics in nonmagnetic materials are described by

$$\frac{\partial \mathbf{S}}{\partial t} = D_s \nabla^2 \mathbf{S} + \gamma \mathbf{B} \times \mathbf{S} - \frac{\mathbf{S}}{\tau_s} + \mathbf{G}, \quad (1)$$

where  $\mathbf{S}$  is the spin density,  $D_s$  is the spin diffusion constant,  $\gamma = g\mu_B/\hbar$  is the gyromagnetic ratio,  $\mathbf{B}$  is the total magnetic field experienced by the spins,  $\tau_s$  is the spin relaxation time, and  $\mathbf{G}$  represents the spin generation term e.g., irradiation with circularly polarized light.  $\mathbf{S}$  is a function of time  $t$  and spatial position  $\mathbf{r} = (x, y)$  for the 2D sample that we consider. While all of the terms can be functions of  $t$  and  $\mathbf{r}$ , we will consider  $\mathbf{B}$ ,  $\mathbf{G}$  and  $\tau_s$  which are independent of  $t$ , and  $D_s$  will be independent of both space and time. The formalism can be readily extended to include electric fields, spin-orbit effects, hyperfine coupling and a third spatial dimension for a more comprehensive treatment. Also, we are usually interested in the *steady-state* solution  $\partial \mathbf{S} / \partial t = 0$ , and the parallel component of  $\mathbf{S}$ ,  $S_{\parallel}$ . We will refer to “parallel” and “perpendicular” with respect to the injected spin direction. Experimentally  $S_{\parallel}$  is the most commonly measured quantity. However, it should be noted that we can evaluate any component of the spin in our simulations.

If  $\mathbf{B}$  and  $\tau_s$  are *position-independent*, the steady-state differential equation can be solved by Fourier transform providing analytical expressions which are helpful for understanding the more complex case where  $\mathbf{B}$  varies in

space. In the steady state, the Fourier-transformed equation for the spin density  $\mathbf{S}(\mathbf{k})$  takes the form

$$-k^2 D_s \mathbf{S}(\mathbf{k}) + \gamma \mathbf{B} \times \mathbf{S}(\mathbf{k}) - \mathbf{S}(\mathbf{k})/\tau_s + \mathbf{G}(\mathbf{k}) = 0 \\ \Rightarrow \mathbf{S}(\mathbf{k}) = [(k^2 D_s + \tau_s^{-1})I - \mathcal{B}]^{-1} \mathbf{G}(\mathbf{k}) \quad (2)$$

where  $\mathbf{S}(\mathbf{k})$  and  $\mathbf{G}(\mathbf{k})$  are vectors.  $I$  is the  $3 \times 3$  unit matrix. We introduce the  $3 \times 3$  matrix  $\mathcal{B}$  with elements  $\mathcal{B}_{xx} = \mathcal{B}_{yy} = \mathcal{B}_{zz} = 0$ ,  $\mathcal{B}_{xy} = -\mathcal{B}_{yx} = \gamma B_z$ ,  $\mathcal{B}_{yz} = -\mathcal{B}_{zy} = \gamma B_x$ ,  $\mathcal{B}_{zx} = -\mathcal{B}_{xz} = \gamma B_y$ . The real-space spin density is then given by the inverse Fourier transform of  $\mathbf{S}(\mathbf{k})$ .

An important case experimentally is given by the globally averaged spin polarization  $\mathcal{H}_g = \int_A S_{\parallel}(\mathbf{r}) d^2 r / [\tau_s \int_A G_{\parallel}(\mathbf{r}) d^2 r]$ , where the area of integration,  $A$ , extends over the entire space, for  $\mathbf{G} = G_{\parallel} \hat{\parallel}$ . Note that  $\mathcal{H}_g \propto S_{\parallel}(k=0)$  and thus from Eq. 2 is independent of  $D_s$  and is given by

$$\mathcal{H}_g = \frac{1}{1 + \theta_B^2} \quad (3)$$

where  $\theta_B$  is an effective *dephasing factor* given by

$$\theta_B^2 = \frac{\gamma^2 B_{\perp}^2 \tau_s^2}{1 + \gamma^2 B_{\parallel}^2 \tau_s^2} \quad (4)$$

Spins precess in a cone whose opening half-angle is that between the total vector magnetic field and the injected spin orientation (see inset, Fig. 1). In combination with this precession, the continuous injection of spins causes a distribution of phases, relative to  $\hat{\parallel}$ , weighted by the spin lifetime. A parallel field reduces the cone opening angle resulting in a spin ensemble more aligned with the injected spin direction, while  $B_{\perp}$  has the opposite effect. The dephasing factor  $\theta_B$  (representing the competition between parallel and transverse fields) describes the projection of spins along the injection axis and the behavior of  $\mathcal{H}_g$ .

$\mathcal{H}_g$  is used experimentally to provide insight into spin lifetime. One can plot the *global* Hanle curve,  $\mathcal{H}_g$  as a function of a field  $\mathbf{B}_h$  applied transverse to the injected spin direction. Here we take  $\hat{\parallel}$  to be  $\hat{x}$  or  $\hat{z}$  and  $\mathbf{B}_h = B_h \hat{y}$ . In the absence of any other fields  $\mathcal{H}_g(B_h)$  is a Lorentzian with half-width given by  $1/\gamma\tau_s$ . However, in the presence of an additional field this is no longer true. Eqs. 3 and 4 provide the correct solution even when a spatially uniform magnetic field  $\mathbf{B}_u$  is present in addition to  $\mathbf{B}_h$ ; then  $\mathbf{B} = \mathbf{B}_u + \mathbf{B}_h$ . In Fig. 1 we present  $\mathcal{H}_g$  calculated in the presence of a spatially uniform field,  $\mathbf{B}_u = B_x \hat{x} + B_y \hat{y} + B_z \hat{z}$  with the spins injected along the  $\hat{z}$  direction for various  $\mathbf{B}_u$  and use the unitless parameter  $\gamma\tau_s B_h$  on the bottom axis. The half-width at half-maximum  $B_{1/2}$  for a general  $B_u$  is given by  $\gamma\tau_s B_{1/2} = \sqrt{1 + \gamma^2 \tau_s^2 (B_x + B_z)^2}$ . A transverse field  $B_x$  reduces  $\mathcal{H}_g(B_h = 0)$  (blue curve) and  $B_h \sim B_x$  is required to significantly reduce  $S_z$  further. A non-zero  $B_{\parallel}$

(red curve) on the other hand will not reduce  $\mathcal{H}_g(B_h = 0)$  but will broaden the Hanle curve, since  $B_h \sim B_z$  is required to significantly increase the precession cone angle and  $\theta_B$ . A field  $B_y$  (parallel to  $B_h$ ) shifts the peak of the Hanle curve, since  $\mathcal{H}_g$  is maximized when the *total* transverse field is zero (black curve). Multiple field components result in a superposition of these effects (green curve).

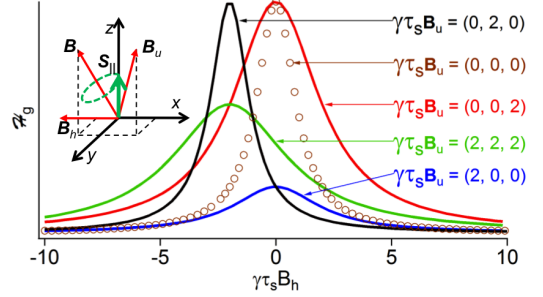


Figure 1: [Color online] Global Hanle curves for various cases of spatially uniform magnetic fields,  $\mathbf{B}_u$ , applied in addition to the swept Hanle field,  $\mathbf{B}_h$ .

The experimentally relevant situation will usually involve spatially varying fields. If  $\mathcal{B}$  is position-dependent and  $D_s \neq 0$ , Eq. 1 cannot be solved analytically in real or Fourier space for steady-state. We have found that solving the original *time-dependent equation* numerically using an Euler method works well for this problem. In this approach, we start from some initial condition,  $\mathbf{S}(\mathbf{r}, t = 0)$ , then iterate in time using a time step  $\Delta t$ , according to the relation

$$\mathbf{S}(\mathbf{r}, t + \Delta t) = \mathbf{S}(\mathbf{r}, t) + \Delta t \times \\ [D_s \nabla^2 \mathbf{S}(\mathbf{r}, t) + \gamma \mathbf{B}(\mathbf{r}) \times \mathbf{S}(\mathbf{r}, t) - \mathbf{S}(\mathbf{r}, t)/\tau_s + \mathbf{G}(\mathbf{r})] \quad (5)$$

The Laplacian is evaluated numerically on a spatial grid of points separated by a suitable distance  $\Delta x$ , and is approximated as  $\nabla^2 \mathbf{S}(\mathbf{r}, t) \sim \frac{1}{(\Delta x)^2} \sum_{\hat{\delta}} [\mathbf{S}(\mathbf{r} + \Delta x \hat{\delta}, t) - \mathbf{S}(\mathbf{r}, t)]$  where  $\hat{\delta}$  represents the unit vectors along the spatial grid. We iterate until  $\mathbf{S}$  does not change appreciably with time. We have verified that the analytical results from the previous section are reproduced by this method. Several experimental global and spatially localized Hanle curves measured under varying conditions can also be qualitatively reproduced [3, 6].

We now use this numerical method to calculate the steady-state distribution of spin density in the presence of a dipolar magnetic field. We consider a dipole having a magnetic moment  $\mathbf{m} = m_z \hat{z}$  located at  $(0, 0, z_t)$ , where the sample lies in the  $xy$ -plane. For a point dipole approximation,  $\mathbf{B}_{dip}(x, y) = \frac{\mu_0}{4\pi} [(3\mathbf{R}(\mathbf{m} \cdot \mathbf{R}) - \mathbf{m}R^2)/R^5]$ , where  $\mathbf{R} = x\hat{x} + y\hat{y} + z_t\hat{z}$  and  $\mu_0$  is the permeability of free space.

Panel (a) of Fig. 2 shows the spatial variation of the steady-state spin density  $S_z$  (left axis) in the presence of

the dipolar tip field assuming uniform injection ( $\mathbf{G} = G_0 \hat{z}$ ). We present simulated  $S_{\parallel}$  for both  $D_s = 0$  and  $D_s \neq 0$  along with a plot of  $\theta_B$  (right axis) as a function of position for a dipole field. The clear correlation between  $S_{\parallel}$  and  $\theta_B$  for  $D_s = 0$  follows naturally from Eq. 3, since spins remain stationary in the absence of diffusion and experience a uniform field:  $S_{\parallel}(r) = \tau_s G_{\parallel}(r) / [1 + \theta_B^2(r)]$ . Turning on diffusion smears out the sharp features. In particular if the minima in  $S_{\parallel}$  (for  $D_s = 0$ ) occur less than a spin-diffusion length  $L_s$  away from the central peak, then the peak will collapse causing a hole in the spin density. Panel (b) of the figure shows Hanle curves with and without diffusion for different Gaussian generation functions  $\mathbf{G} = G_z \exp(-2r^2/r_g^2) \hat{z}$ , where  $r_g$  is the radius of the Gaussian. The key feature to note is that as the generation radius decreases, a higher percentage of spins experience strong  $B_{\parallel}$  from the tip field and  $\mathcal{H}_g$  is substantially broadened. The dip at  $\mathbf{B}_h = 0$  for  $D_s \neq 0$ ,  $r_g/z_t < 1$  occurs when a significant number of spins experience nonzero  $B_y$  as they diffuse away from the injection area in the center.

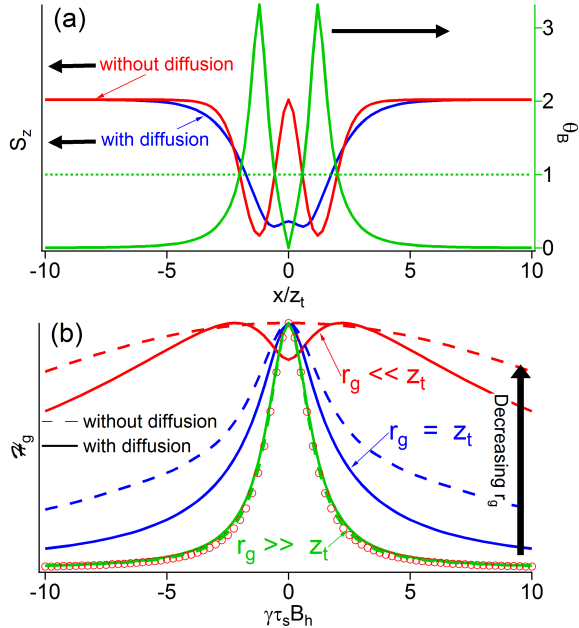


Figure 2: [Color online] a) Steady state spin density  $S_z(x/z_t, y = 0)$  in the presence of a dipole field for  $D_s = 0$  (red) and  $D_s \tau_s / z_t^2 = 1$  (blue). The dipole  $m_z \hat{z} (\frac{\mu_0 m_z}{\pi z_t^3} = 10)$  is located at  $\mathbf{r}/z_t = (0, 0, 1)$  and uniform injection is assumed. The green curve shows the spin dephasing factor  $\theta_B(x)$ ; note that  $\theta_B = 1 \Rightarrow S_z = 0.5$  for  $D_s = 0$ . b) Global Hanle curves, with and without diffusion, for different Gaussian generation functions. The dashed lines correspond to  $D_s = 0$  case, while the solid lines are for  $D_s \tau_s / z_t^2 = 1$ . Green, blue and red curves correspond respectively to  $r_g/z_t \gg 1$  (uniform injection),  $= 1$ , and  $< 1$ . For comparison, the circles show the Hanle assuming no dipole tip.

Fig. 2 shows that a dipole magnetic field creates local-

ized features in the spin density  $S_z$  with a characteristic length scale given by the dipole-sample separation  $z_t$ . This suggests the possibility of using a scanned dipole as a tool for imaging spin density features with a resolution set roughly by this separation.

Fig. 3 demonstrates this concept by considering a sample which has a small localized region in which the spin lifetime is five times shorter than the rest of the sample (inside the dashed white line). If the magnetic dipole is held directly above this region, the resulting spin density will be distributed as shown in panel (a) of the figure. Panel (b) shows  $\mathcal{H}_g$  as a function of the relative position of the dipole. Short-lived spins are more difficult to dephase because they relax before they can precess. Since the dipole field selectively dephases a small area of spins, the global average spin density of the sample will be larger when the dipole affects the region of short  $\tau_s$ . By scanning the dipole tip in the  $xy$ -plane and measuring the global spin density (a measurement which ordinarily has a spatial resolution set by the “global” area from which the signal is collected, whether optically or electrically), local variations of  $\tau_s$  can be detected. The image resulting from such an experiment is shown in panel (b) of Fig. 3.

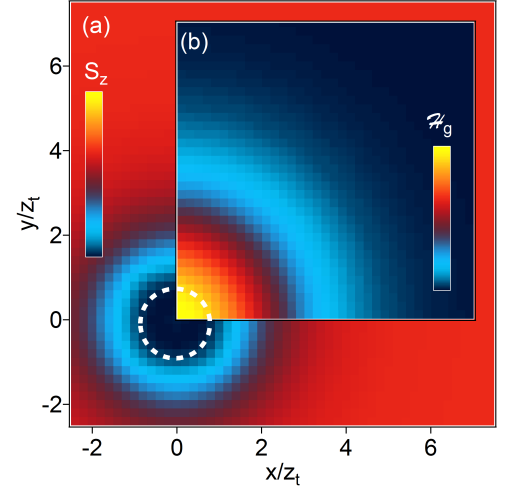


Figure 3: [Color online] Demonstration of the ability to image local properties using global measurements: embedded in a uniform plane is a small region (bounded by the white dotted circle) in which  $\tau_s$  is five times smaller than throughout the remaining area. The 2D sample is uniformly pumped with spins. (a) Spatial map of the local value of  $S_z(\mathbf{r})$  when the tip is centered over the reduced  $\tau_s$  region (at  $(0,0)$ ). (b)  $S_z$  integrated over the entire sample as a function of the location of the dipole tip relative to the region of reduced  $\tau_s$ .

Given any magnetic field spatial profile, our numerical method is capable of producing the resulting steady-state spin density. In particular, it can simulate the impact of magnetic fields with random spatial variation. Such fields have gained attention in electrical injection devices

([13–15]) which have shown experimental evidence for the impact of inhomogeneous magnetic fields on Hanle measurements. Fig. 4 shows calculated Hanle curves in the presence of random magnetic fields. We consider a field  $\mathbf{B}_r = \mathcal{N}(0, B_v)\hat{x} + \mathcal{N}(0, B_v)\hat{y} + \mathcal{N}(0, B_v)\hat{z}$  where we sample a normal distribution of mean zero and variance  $B_v$  for each field component at every spatial point. We present for three cases of  $B_v : \ll 1/\gamma\tau_s, = 1/\gamma\tau_s$ , and  $> 1/\gamma\tau_s$ . When these random fields become comparable to or greater than  $1/\gamma\tau_s$  the Hanle curves are significantly broadened; clearly these effects can confound the determination of spin lifetimes from Hanle widths. While the actual stray field from a rough ferromagnetic injector needs to be calculated carefully by taking into account the experimental device characteristics (roughness, saturation magnetization, domain size, thickness, etc.), stray fields of the order kilogauss are readily achievable a few nanometers away from a rough injector.

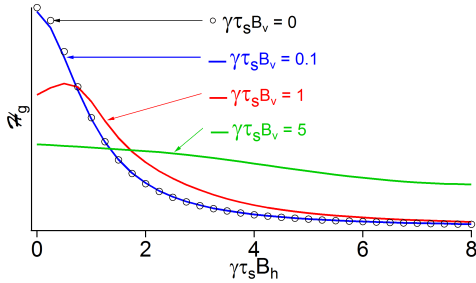


Figure 4: [Color online] Global Hanle curves for a sample with randomly spatially varying magnetic field,  $\mathbf{B}_r = \mathcal{N}(0, B_v)\hat{x} + \mathcal{N}(0, B_v)\hat{y} + \mathcal{N}(0, B_v)\hat{z}$ . Such fields may be expected in electrical injection devices with rough injectors. The injected spins are assumed to be along the x-axis in this simulation.

We have presented a means of solving the partial differential equation describing spin dynamics in a thin non-magnetic layer in the presence of an inhomogeneous magnetic field (such as that of a micromagnetic tip for scanned probe force detection or an imperfect ferromagnetic injector). Our approach can be used to unify the analysis of a range of experiments performed under varying conditions, and resulting Hanle curves can be understood in detail. Notably, significant broadening occurs for fields parallel to the injected spin orientation. This mechanism can be especially important in electrical spin injection devices; hence care must be taken in deducing spin lifetimes from Hanle curve widths. We have also proposed a new technique for imaging spin properties of spatially inhomogeneous materials by relying on the localized spin density features generated by a dipole field.

We gratefully acknowledge enlightening discussions with Ron Jansen. This work was supported by National Science Foundation through the Materials Research Science and Engineering Center at The Ohio State University (DMR-0820414) and Department of Energy, Office of Science (DE-FG02-03ER46054).

---

\* Electronic address: hammel@mps.ohio-state.edu

- [1] I. Žutić, J. Fabian, and S. D. Sarma, *Rev. Mod. Phys.* (2004),
- [2] D. D. Awschalom and M. E. Flatte, *Nature Phys.* **3**, 153 (2007), ISSN 1745-2473,
- [3] F. Jedema, H. Heersche, A. Filip, J. Baselmans, and B. van Wees, *Nature* **416**, 713 (2002)
- [4] S. Crooker, M. Furis, X. Lou, C. Adelmann, D. Smith, C. J. Palmstrom, and P. A. Crowell, *Science* **309**, 2191 (2005),
- [5] X. Lou, C. Adelmann, S. A. Crooker, E. S. Garlid, J. Zhang, K. S. M. Reddy, S. D. Flexner, C. J. Palmstrom, and P. A. Crowell, *Nature Phys.* **3**, 197 (2007),
- [6] M. Furis, D. L. Smith, S. Kos, E. S. Garlid, K. S. M. Reddy, C. J. Palmstrom, P. A. Crowell, and S. A. Crooker, *New J. Phys.* **9**, 347 (2007),
- [7] T. Sasaki, T. Oikawa, T. Suzuki, M. Shiraishi, Y. Suzuki, and K. Noguchi, *IEEE Trans. Magn.* **46**, 1436 (2010),
- [8] T. Sasaki, T. Oikawa, T. Suzuki, M. Shiraishi, Y. Suzuki, and K. Noguchi, *Appl. Phys. Lett.* **96**, 122101 (2010),
- [9] K. Pi, W. Han, K. M. McCreary, A. G. Swartz, Y. Li, and R. K. Kawakami, *Phys. Rev. Lett.* **104**, 187201 (2010),
- [10] B. Huang and I. Appelbaum, *Phys. Rev. B* **77**, 165331 (2008),
- [11] I. Appelbaum, B. Huang, and D. J. Monsma, *Nature* **447**, 295 (2007), ISSN 0028-0836,
- [12] H. C. Koo, J. H. Kwon, J. Eom, J. Chang, S. H. Han, and M. Johnson, *Science* **325**, 1515 (2009),
- [13] S. P. Dash, S. Sharma, R. S. Patel, M. P. de Jong, and R. Jansen, *Nature* **462**, 491 (2009), supplementary information,
- [14] C. Awo-Affouda, O. M. J. van 't Erve, G. Kiioseoglou, A. T. Hanbicki, M. Holub, C. H. Li, and B. T. Jonker, *Appl. Phys. Lett.* **94**, 102511 (2009),
- [15] R. Jansen (2010), *Novel Magnetic Materials International Workshop*.
- [16] F. Meier and B. P. Zakharchenya, *Optical Orientation* (North-Holland, 1984), ISBN 9780444867414.
- [17] C. H. Li, G. Kiioseoglou, O. M. J. van 't Erve, P. E. Thompson, and B. T. Jonker, *Appl. Phys. Lett.* **95**, 172102 (2009),
- [18] Y. Ando, K. Hamaya, K. Kasahara, Y. Kishi, K. Ueda, K. Sawano, T. Sadoh, and M. Miyao, *Appl. Phys. Lett.* **94**, 182105 (2009),
- [19] O. M. J. van 't Erve, A. T. Hanbicki, M. Holub, C. H. Li, C. Awo-Affouda, P. E. Thompson, and B. T. Jonker, *Appl. Phys. Lett.* **91**, 212109 (2007),